fractal and fractional

MDPI

Article

Measurement of 2D and 3D Fractal Features of Urban Morphology from an Architectural View and Its Influencing Factors

Chenming Zhang [1,*], Xiaoying Ping [2], Qindong Fan [1] and Chunlin Li [3]

[1] College of Architecture, North China University of Water Resources and Electric Power, Zhengzhou 450046, China; qindongf@ncwu.edu.cn
[2] School of Public Administration, North China University of Water Resources and Electric Power, Zhengzhou 450046, China
[3] CAS Key Laboratory of Forest Ecology and Management, Institute of Applied Ecology, Chinese Academy of Sciences, Shenyang 110016, China
* Correspondence: zhangchenming@ncwu.edu.cn

Abstract: Urban morphology has been empirically demonstrated to be self-organized and can be quantified by fractal dimension. However, the spatial variation rule of fractal features at the sub-zone scale has yet to be uncovered, as well as the relationship between fractal dimension values and road network or land-use patterns. In this study, the urban area is partitioned into 158 grid units, with subsequent calculations conducted to determine the fractal dimensions (using 2D box-counting and 3D voxel-counting methods), road network characteristics, and land-use patterns within each individual unit. The pattern of how architectures fill into the 2D or 3D embedding space at the grid level is revealed. Moreover, the spatial relationship between the road network, land-use, and their impacts on the local architectural layout is elucidated by employing MGWR, a model that incorporates the principles of fitting localized spatial regression. The results are as follows: (1) urban morphology follows fractal laws at a sub-zone scale, both in a 2D plane and 3D volume; (2) the filling degree of architecture is high in the urban center but low in the periphery areas; (3) the selected variables fit well with the regression models; (4) there is spatial heterogeneity regarding the influence of each factor. The research findings provide valuable insights into the theoretical relationship between urban morphology and the composite structure of road networks and land use. This facilitates identifying crucial areas and priority directions for urban renewal construction, as well as optimizing architectural design to improve efficiency and functionality.

Keywords: fractal dimensions; box-counting dimension; urban morphology; architecture layout; road network

Citation: Zhang, C.; Ping, X.; Fan, Q.; Li, C. Measurement of 2D and 3D Fractal Features of Urban Morphology from an Architectural View and Its Influencing Factors. *Fractal Fract.* **2024**, *8*, 138. https://doi.org/10.3390/fractalfract8030138

Academic Editor: Palle Jorgensen

Received: 17 January 2024
Revised: 21 February 2024
Accepted: 23 February 2024
Published: 27 February 2024

1. Introduction

Urban morphology exhibits a complicated space-filling process and self-organized pattern. A thorough study of urban morphology starts with its description, followed by an understanding of its organization and working. Conventional geometric measurements of urban features include the perimeter, area, and volume, which are based on a specific scale and defined as a "characteristic scale" [1]. However, urban morphology resembles natural beings, such as coastlines or bacterial colonies, which have no characteristic scale and cannot be precisely depicted by basic measures such as length, area, or volume [2]. Fortunately, fractal geometry provides a powerful method to solve the problem of "no characteristic scale" and can effectively measure scale-free phenomena such as urban form.

Cites can be empirically treated as fractal systems, bearing self-similarity or self-affinity properties [3]. Since Batty [4] developed the "fractal city" theory, the fractal approach—used in understanding urban morphology features and the iterative rules of urban growth

evolution—has become an increasingly important topic in urban science. For example, Benguigui [5] determined the fractal dimension as a function of time using the Tel Aviv metropolis as a case. Feng et al. [6] analyzed the evolutionary characteristic of urban form and land-use structure in Hangzhou, China, and found that self-similarity exists in both the built-up area and the municipal area. Yin et. al. constructed a dynamic fractal framework and applied this theory to study the urbanization of Boston [7]. In these studies, the relationships between fractal cities and self-organization rules are widely reported.

The calculation methods for fractal dimensions play a significant role in fractal studies. There are several common algorithms, including the perimeter–area method, area–radius method, and box-counting method, and each of them corresponds to a specific physical prosperity. The perimeter–area method is derived from Mandelbrot's concepts [8] and is used to depict the fractal characteristic of island-type objects; it has been widely used to represent the shape complexities and irregularities of urban boundaries [9,10]. The area–radius dimension is designed to quantify the agglomeration degree of the built-up area. This method is suited for indicating urban growth, as the key to the algorithm lies in building the relationship between the radius (a scale) from the urban core and the corresponding built-up area (a measurement) [11,12]. The box-counting method measures the spatial filling degree of fractal objects, in other words, it reveals how the space is occupied by complex patterns [13,14]. The conventional box-counting method is commonly employed in a 2D plane to describe the urban spatial structure and texture; further, a 3D voxel-counting method is developed to measure the building morphology embedded into a 3-dimensional space [15].

There can be different types of objects measured to embody fractal urban morphology, from built-up areas to road network structures [16–18]. When the objects are architectures, there exists a spatial correlation between the distribution of architecture and urban morphology [19]. On the one hand, the urban space is composed of various architectures and can be divided into indoor and outdoor spaces, acting as a "figure and ground" complex in urban texture (Figure 1a) [20]. On the other hand, architectures can be considered as "filling clusters" within the framework of urban morphology, which falls into the scope of the box-counting dimension application [21,22]. Further, the box-counting dimension serves as a comprehensive measurement of the spatial unevenness and complexity of the architectural layout [23], and a higher value indicates a more effective and compact urban morphology.

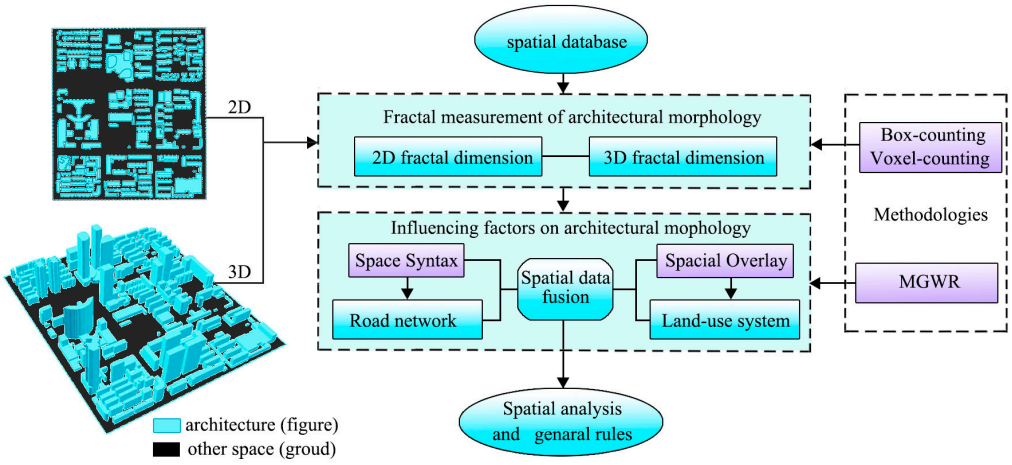

(a) Sample of 2D and 3D architecture groups (b) Flow chart of the research

Figure 1. Graphic of the entire research.

When it comes to the influencing factors of urban morphology, road networks and land-use patterns are found to have deep and complicated effects on urban form. Theoretically, it is well-known that road networks shape the urban framework and organize traffic flow,

and the function of land use determines the building form [24,25]. Moreover, accessibility improvement and increasing land-use mixing levels lead to the development of density-built-up areas with high vitality [26,27]. In terms of methods and practices, space syntax variables are frequently used to assess the different types of accessibility and traffic flow in the road network [28]. The advantage of this method lies in the effective identification of integrated roads and key hubs using the topological connections between different roads as a whole network [29]. The area, density, and proportion distribution of land for different purposes are other types of common indices that identify the intensity of land functions and provide a foundation for urban functional zoning at a community scale [30]. Further, the relationship between different variables can be built up through various regression models, such as the spatial lag model or spatial error model [31,32]. Given that there exists spatial heterogeneity within urban spaces [33], geographically weighted regression (GWR) is increasingly being applied in urban morphology studies [34]. The above provides a theoretical and methodological basis for the study of influencing factors on urban morphology.

Still, there were several limitations in the previous studies:

(1) The 3D voxel-counting fractal dimension model for architectural object measurement remains in the primary stage.
(2) A fine-scaled study on fractal features within urban sub-zones has not been conducted, nor has its visualization.
(3) The relationship between 2D or 3D fractal dimensions as well as their influencing factors, such as road network variables and land-use patterns, have not been explored.

The resolution of the aforementioned issues carries substantial theoretical and practical implications. Firstly, this study contributes to unveiling the functional mechanism underlying the fractal dimension at a subzone level within traffic-land composite systems, providing insights into determining optimal urban morphology. Secondly, it facilitates the effective implementation of urban planning by addressing inherent qualitative limitations associated with conventional approaches. This enables improved alignment between architectural layout and traffic-land systems to enhance efficiency and functionality in shaping urban morphology.

This study uses architectures as fractal objects and conducts fractal measurement within the subzone through 2D and 3D box (voxel)-counting methods, then the fractal features are mapped to obtain a fine-scaled portrait of urban morphology. Finally, a multiscale geographically weighted regression (MGWR) model is established to explore what effects the road network and land-use patterns have on urban morphology (Figure 1b).

2. Study Area, Methodologies and Variables

2.1. Study Area

The city of Zhengzhou is chosen as the case study (Figure 2a). As the provincial capital of Henan, Zhengzhou's metropolis area has a dense and diverse architectural complex, providing a sufficient sample size for supporting urban fractal research. (Fractal research can still be conducted in cities lacking dense and diverse architectural complexes, but the overall fractal dimension may be low, making it challenging to analyze the local spatial variations of fractal dimensions at the subzone level [35]).

The study area is bounded by the outer ring roadways from 113.52 E to 113.82 E and 34.66 N to 34.89 N (Figure 2b). It has a surface area of approximately 56,436 hm^2. The studied area has a polycentric structure with an integrated traffic network made up of grid-like roads and ring roads, which are highly representative of Chinese megacities. Understanding the spatial rules and influencing factors of the architectural morphology of cities with similar structures is greatly facilitated by selecting the downtown area of Zhengzhou as the case study. Based on field research and data preprocessing results, the research area is divided into 158 grids (Figure 2c) as the basic analysis units, and fractal research with fine-scale detail on the architectural form is conducted within these grids.

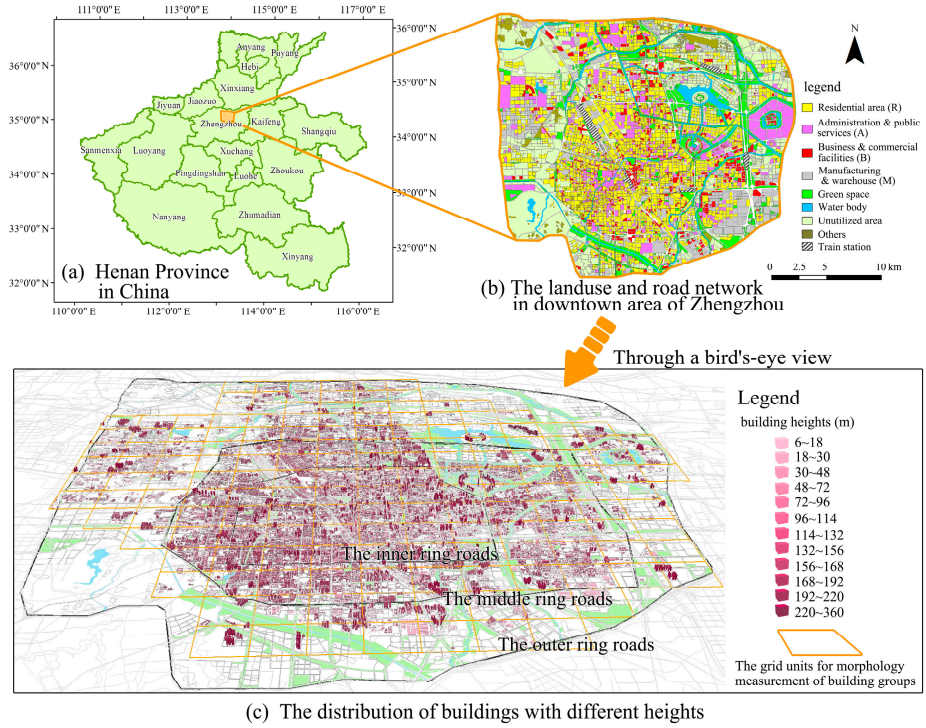

Figure 2. Primary data in the study area.

2.2. *Methodologies*

The flowchart of the methodologies consists of 4 parts, which can be seen as follows Figure 3:

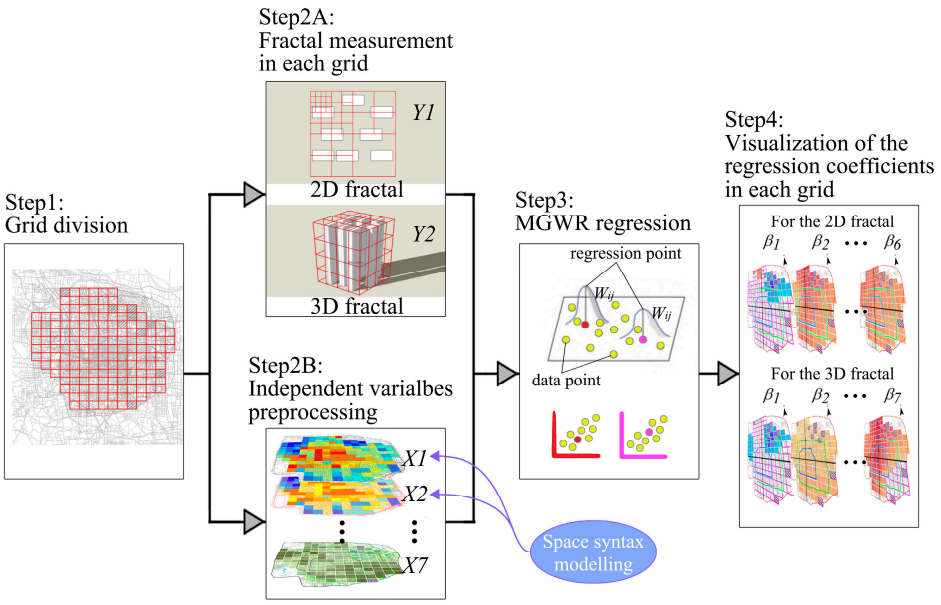

Figure 3. Flowchart of the methodologies.

2.2.1. 2D Fractal Dimension (*2D_FD*) and 3D Fractal Dimension (*3D_FD*)

The computational method for the 2D box-counting dimension (*2D_FD*) and 3D voxel-counting dimension (*3D_FD*) is based on the same idea that space can be measured by units with different scales. The fractal dimension can be calculated by the relationship between the measurement outcomes and the measurement scale. As for *2D_FD*, the architectures are measured by a series of boxes with different sizes. When the size of the "box units" is

set as r, the number of "box units" required to cover all the architectures is $N(r)$. Then, the relationship between r and $N(r)$ should obey the law as follows:

$$N(r) \propto r^{-FD} \tag{1}$$

In Equation (1), FD is the fractal dimension.

After the $N(r)$ values are obtained, lg$r$ and lg$N(r)$ are plotted as the abscissa and ordinate, respectively, and the regression line equation can be built as follows [36]:

$$\lg N(r) = -FD\lg r + \lg k \tag{2}$$

In Equation (2), k is a constant and lg$k$ serves as the intercept of the regression line, FD is the fractal dimension that represents the negative value of the slope of the regression line and it depicts the complexity and regularity of the architecture morphology.

The measurement units in the *2D_FD* case are 2D boxes, while in the *3D_FD* case, they are 3D voxels. Taking the 3-dimension, for example, assuming that the 3D urban space is M, it can be completely enclosed by its bounding cuboid with dimensions featuring the length, L, width, W, and height, H. This $L \times W \times H$ cuboid serves as the ruler, with its scale denoted as $r_1 = L$. It is evident that the number of cuboids required to enclose all architectures within space M (equivalent to the number of non-empty cuboids) should be $N(r_1) = 1$.

Subsequently, the cuboid is equally divided into eight voxels with dimensions of $L/2 \times W/2 \times H/2$ with its scale denoted as $r_2 = L/2$. The number of voxels required to encase all architectures within space M is then calculated as $N(r_2)$. Similarly, this process continues for smaller voxel sizes, such as $L/4 \times W/4 \times H/4$, with a corresponding scale of $r_3 = L/4$. The number of voxels required at each step follows this pattern.

Following this progression, the size of the voxel ruler gradually decreases proportionally. At step n, where $r_n = L/2^{n-1}$, we record the number of non-empty voxels needed to encase all architectures in space M as $N(r_n)$. If the architectural morphology in space M exhibits fractal characteristics, the scale's r value and its corresponding non-empty voxel number $N(r)$ should conform to Formula (1), enabling computation of the *3D_FD* value using Formula (2).

2.2.2. Space Syntax Modelling

Space syntax is used to estimate two types of traffic flow (namely, through-movement and to-movement) based on the topology network theory. *Choice* and *Integration* are the most common variables measuring the two aforementioned indexes [29].

The *Choice* index is used to calculate the number of times that a certain road segment appears on the shortest path from any origin to any destination, representing the possibility that the road is chosen. The higher the *Choice* index value is, the more through-movement traffic on the correlating roads, which indicates more vehicles and people passing by. The *Choice* can be calculated as follows:

$$Choice = \frac{\log\left[\frac{\sum_{i=1}^{n}\sum_{j=1}^{n}\sigma(i,x,j)}{(n-1)(n-2)} + 1\right]}{\log\left[\sum_{i=1}^{n} d(x,i) + 3\right]}, i \neq j \tag{3}$$

In Formula (3), n is the total number of road segments; $d(x, i)$ is the shortest distance from x to i, and $\sigma(i, x, j)$ is the shortest distance from i to j through x. When the trajectory from i to j passes through x, $\sigma(i, x, j) = l(i)l(j)$; when $I \neq x = j$ or $I = x \neq j$, $\sigma(i, x, j) = l(i)l(j)/2$; when the trajectory from i to j does not pass through x, $\sigma(i, x, j) = 0$.

The *Integration* index is used to measure the connection and accessibility, reflecting the attractiveness of socioeconomic activities. The higher the *Integration* index value, the more

to-movement traffic on the correlating roads, indicating more vehicles and people arriving. The *Integration* can be calculated as follows [37]:

$$\begin{cases} Integration = \frac{RA(a_x)}{D_n} \\ \text{Where : } RA(a_x) = \frac{n(log((n+2)/3)-1)+1}{(n-1)(n-2)/2},\ D_n = \frac{2(MD(a_x)-1)}{n-2} \end{cases} \quad (4)$$

In Formula (4): n is the total number of road segments in the road network system, and MD (a_x) is the mean depth of road segment a_x.

2.2.3. MGWR

MGWR is derived from GWR; both are typical local regression models that allow the parameters to vary spatially and are different from the conventional global regression models, which assume that the coefficients to be estimated are constant over space [38,39].

In the GWR model, the spatial locations of the sample data are considered parameters in the coefficient estimation; the calculation formula is as follows:

$$y_i = \beta_{i1}(u_i, v_i)\ x_{i1} + \beta_{i2}(u_i, v_i)\ x_{i2} \ldots\ldots \beta_{i7}(u_i, v_i)\ x_{i7} + \beta_{i0} + \varepsilon_i \quad (5)$$

In formula (5), (u_i, v_i) is the geographic coordinate of the center point in the ith grid sample; y_i is the dependent variable representing the *2D_FD* or *3D_FD* value of grid i; $(x_{i1}, x_{i2} \ldots\ldots x_{i7})$ denotes the vector of the independent variables in grid i, which will be explained in Section 2.3. β_{i0} and ε_i are the intercept and random error in grid i. $(\beta_{i1}(u_i, v_i)$, $\beta_{i2}(u_i, v_i) \ldots\ldots \beta_{i7}(u_i, v_i))$ is the vector of regression coefficients to be estimated for grid i, which can be estimated as follows:

$$(\hat{\beta}_{i1}(u_i, v_i)\ , \hat{\beta}_{i2}(u_i, v_i)\ \ldots\ldots \hat{\beta}_{i7}(u_i, v_i)\ )^T = [X^T W(u_i, v_i) X]^{-1} X^T W(u_i, v_i) Y \quad (6)$$

$W(u_i, v_i)$ is the spatial weight matrix, which is set up by the bi-square method [40].

As an improvement to the GWR model, the MGWR model allows relationships between dependent and independent variables to vary at different scales. In the MGWR model, the most suitable bandwidth is searched for and acquired to avoid the mismatch between bandwidth and parameter estimation for particular samples. As a result, the scale effects and spatial variation of the influence on urban morphology can be better understood. The computation method is as follows:

$$y_i = \sum_{j=1}^{k} \beta_{bwi}(u_i, v_i)\ x_{ij} + \varepsilon_i \quad (7)$$

In Formula (7), *bwi* is the bandwidth of the ith grid, β_{bwi} is the regression coefficient of the jth independent variable in grid i when setting *bwi* as the bandwidth, the other variables have the same meaning as in Formula (5).

The regression model can be conducted by the mgwr-2.2.1 software accessed from "https://sgsup.asu.edu/sparc/multiscale-gwr" (accessed on 7 October 2023).

2.3. Variable Selection and Mapping

As well-known, the layout of architectural groups will be affected by urban streets and land-use systems, so the 2D and 3D fractal dimensions of architectural groups are regarded as dependent variables, and the road network and land use proportion are regarded as independent variables. The computed values and spatial distributions of 2D and 3D fractal dimensions will be displayed as results in Section 3.1 while the mappings of independent variables will be shown as data preparations in this section.

In terms of the road network, the *Choice* index is selected as *X1* to estimate the traffic flow of "through-movement" (e.g., a higher *Choice* index value corresponds with more through-movement trajectories in segment AB, Figure 4a). The *Integration* index is selected as *X2* to estimate the traffic flow of "to-movement" (e.g., a higher *Integration* index value

corresponds with more to-movement trajectories in segment AB, Figure 4b). According to pertinent research, there is a significant correlation of 70% between the aforementioned indicators and their corresponding actual traffic flow [41]; the distributions of "through-movement" and "to-movement" are mapped in Figure 4c,d, respectively. Finally, the node number of the road network is counted in each grid and defined as *X7*, which is mapped in Figure 5e.

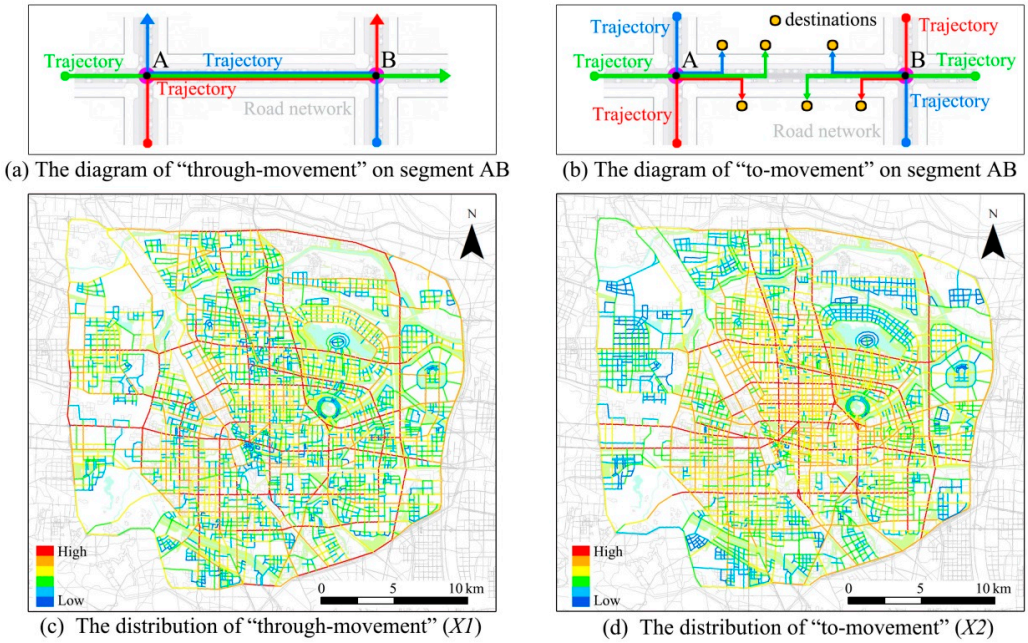

(a) The diagram of "through-movement" on segment AB (b) The diagram of "to-movement" on segment AB

(c) The distribution of "through-movement" (*X1*) (d) The distribution of "to-movement" (*X2*)

Figure 4. The distribution of two types of traffic movement.

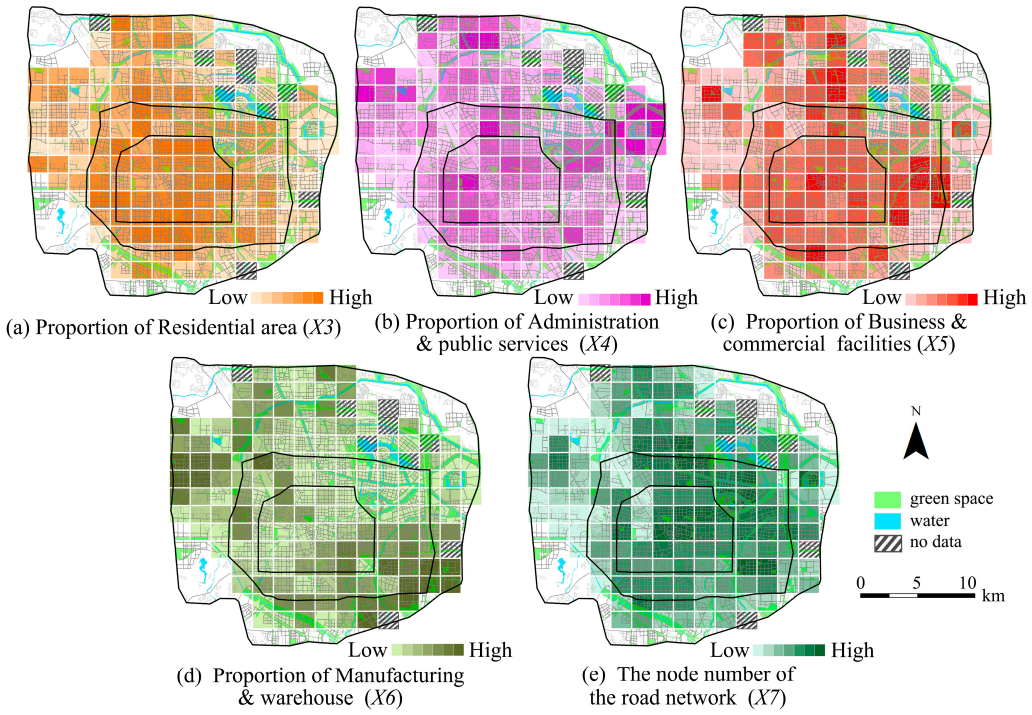

(a) Proportion of Residential area (*X3*) (b) Proportion of Administration & public services (*X4*) (c) Proportion of Business & commercial facilities (*X5*)

(d) Proportion of Manufacturing & warehouse (*X6*) (e) The node number of the road network (*X7*)

Figure 5. The distribution of variables from X1 to X7.

In terms of land use, the proportion of the residential area is selected as *X3* to estimate the level of residential functionality. The proportion of administration and public areas

is selected as *X4* to estimate the development level of these facilities. The proportion of business and commercial areas is selected as *X5* to estimate the business vitality. The proportion of manufacturing, industrial, and warehouse areas is selected as *X6* to estimate the industrial development level. Each land patch possesses distinct functional attributes and well-defined spatial boundaries, devoid of any inaccuracies. The relative proportions of different land areas within each grid can be determined by overlaying the vectorized land-use map (Figure 2b) onto the 158 grids spatially (Figure 5a,d).

3. Results and Analysis

3.1. The Measurement Results of Fractal Dimensions

3.1.1. The Fractal Measurement of Typical Grids

Different spatial samples are featured with different architectural layouts, corresponding to different fractal dimension values. The purpose of this section is to establish the correspondence between fractal dimensions and their visualized presentations and to portray urban morphology more vividly. Therefore, four typical grids representing different development patterns are selected as samples (Figure 6), in which urban morphology is compared through *2D_FD* and *3D_FD* values.

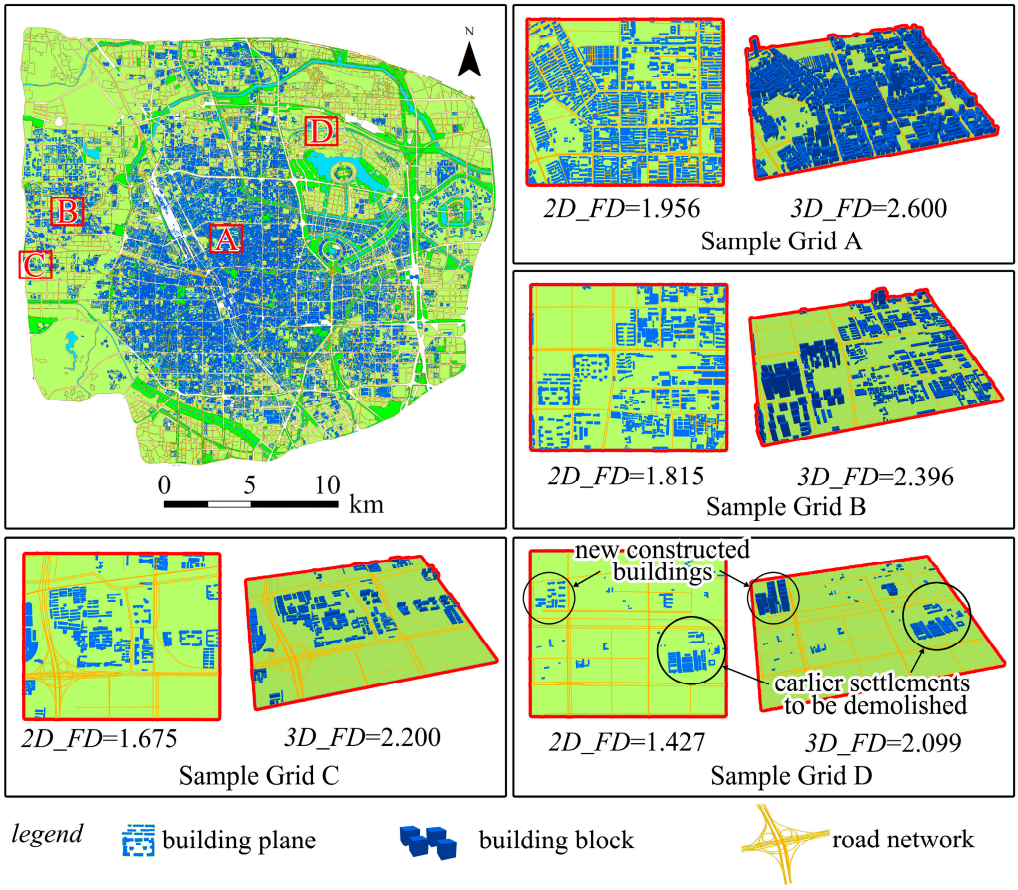

Figure 6. The fractal dimension measurements of a typical architectural group.

From the grid A to grid D samples, the architectures become increasingly sparse and unevenly distributed, with the *2D_FD* and *3D_FD* values decreasing. The specific analyses are as follows:

The grid A sample represents the central cluster of the downtown area, characterized by dense buildings, intensive development, and a few empty spaces. The 2D outline shape of the architecture is regular, with a high filling degree, presenting spatial accordance with the road network structure. The 3D morphology of the architecture appears elevated and

features significant bulk characteristics. These morphological features result in high values of *2D_FD* and *3D_FD* indices.

The grid B sample represents the built-up enclaves, which are separated from the central cluster by a wide corridor of green space or transportation. These areas feature relatively developed urban functions but lower construction intensity than the urban center, with an inferior architecture filling degree compared to the type A sample. These morphological features result in medium values of *2D_FD* and *3D_FD* indices.

The grid C sample represents the urban edge, characterized by a sparse density of architectures and a mismatch between the architectural layout and road network framework. In these places, both regular and irregular architectural groups coexist, with most buildings being low-rise. These morphological features result in relatively low values of *2D_FD* and *3D_FD* indices.

The grid D sample represents the vacant place to be developed, where the road network has just been formed but the new planned buildings have not yet been "filled" into the urban framework. In these areas, the architectural groups are sparse and unevenly distributed. High-rise buildings that have already been built stand within a few plots, and some other low and shabby buildings are clustered within earlier settlements to be demolished. These features result in the lowest values of *2D_FD* and *3D_FD* indices.

It can be deduced that the relationship between the physical architectural conditions in Zhengzhou and the *2D_FD* and *3D_FD* values can be established. The higher the fractal dimension, the denser and more balanced the distribution of buildings, and the more effective the layout of architectural groups in space utilization.

3.1.2. Visualization and Zoning Statistics of Fractal Dimensions

The *2D_FD* and *3D_FD* values of the 158 grids are computed and mapped in Figure 7a to obtain an overall grasp of urban form; the boxplot graphics of different partitions are drawn in Figure 7b for morphological comparisons between different directions and different layers of the city.

In general, urban morphology represents fractal self-similarity at the grid level both in 2D and 3D spaces and conforms to the basic laws of fractal geometry. The *2D_FD* varies within the range of 1 to 2, with the highest value being 1.977 and the lowest value being 1.147; the *3D_FD* varies within the range of 2 to 3, with the highest value being 2.600 and the lowest value being 2.000.

There are different fractal characteristics between the four directions. The medium level of the *2D_FD* distribution presents NE < NW < SE < SW; and the *3D_FD* distribution presents NW < NE < SE < SW. The distribution pattern of *2D_FD* and *3D_FD* values in the SW direction is different from the other three directions. In the SW direction, most samples have high values; other samples have low values and deviate significantly from the median, showing a negatively skewed distribution and the highest medium value. This numerical characteristic corresponds to an abrupt change in the architectural pattern near the city border in this direction in the physical circumstance.

There are different fractal characteristics between the three layers. For example, *2D_FD* and *3D_FD* both present the outer layer < the middle layer < the inner layer. The inner layer is the central core of the downtown where architecture is densely and evenly distributed with an intensive filling pattern. The middle layer serves as a transitional layer that reflects the spatial process of urban expansion, where the fractal dimensions display radius diffusion from the urban center to the periphery. The outer layer is at the forefront of urban expansion, where the built-up enclaves, the suburban areas, and the areas under construction are distributed in a staggered manner, resulting in a heterogeneity of urban morphology.

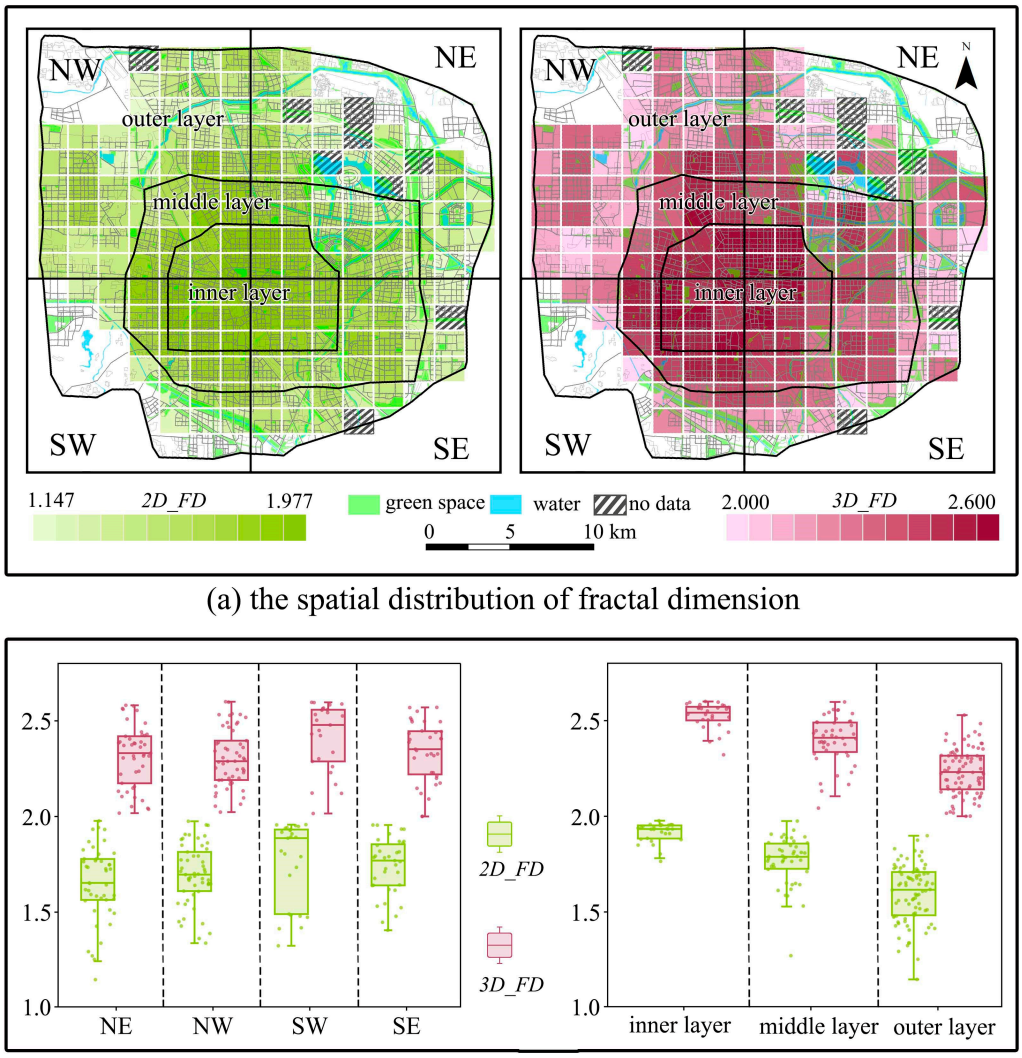

Figure 7. The distribution of *2D_FD* and *3D_FD*.

3.2. The MGWR Results Revealing the Influencing Factors on Fractal Dimensions

3.2.1. General Effect of the MGWR Regression

The regression model is established by using the indexes described in Section 2.3 as independent variables, and *2D_FD* and *3D_FD* as dependent variables, respectively. The multicollinear test for all the independent variables has been passed before conducting the MGWR model, as the VIFs (variance inflation factors) for all independent variables are all below 5.0, meeting the basic conditions for regression. The model fitness results are demonstrated in Table 1, while the statistics of the regression results are shown in Table 2.

From Table 1, the fitting effect of MGWR is much better than those of the conventional OLS and GWR regression models. The MGWR regression obtains lower *RSS*, *AIC*, and *AICc* values and higher R^2 and *Adjusted* R^2 values in both the *2D_FD* and *3D_FD* cases, reflecting the advantages of a stronger explanation for the dependent variable in MGWR compared to traditional regression models. Moreover, the *2D_FD* case obtains lower *RSS*, *AIC*, and *AICc* values and higher *R2* and *Adjusted R2* compared to the *3D_FD* case. In other words, the 2D architectural pattern can be more easily explained by the independent variables compared to 3D morphology.

Table 1. The regression results of different models.

Model Parameter	Results of *2D_FD* Model			Results of *3D_FD* Model		
	OLS Regression	**GWR Regression**	**MGWR Regression**	**OLS Regression**	**GWR Regression**	**MGWR Regression**
RSS	49.692	31.099	25.001	51.430	33.743	28.982
AIC	279.619	251.010	224.071	287.050	259.984	239.572
AICc	282.586	265.355	242.779	290.266	272.341	253.762
R^2	0.685	0.803	0.842	0.674	0.786	0.817
Adjusted R^2	0.673	0.759	0.800	0.659	0.743	0.776

Table 2. Descriptive statistics of the coefficients of the MGWR model.

Dependent Variable: 2D_FD						*Dependent Variable: 3D_FD*					
Variable	**Mean**	**STD**	**Min**	**Median**	**Max**	**Variable**	**Mean**	**STD**	**Min**	**Median**	**Max**
Intercept	0.048	0.177	−0.377	0.04	0.366	*Intercept*	−0.004	0.171	−0.39	0.020	0.349
X1	−0.08	0.145	−0.458	−0.076	0.29	*X1*	−0.146	0.123	−0.489	−0.120	0.086
X2	0.263	0.044	0.185	0.260	0.367	*X2*	0.295	0.069	0.142	0.300	0.420
X3	0.537	0.128	0.222	0.535	0.808	*X3*	0.507	0.008	0.495	0.505	0.521
X4	0.257	0.049	0.178	0.258	0.329	*X4*	0.153	0.083	0.032	0.137	0.295
X5	0.249	0.012	0.228	0.247	0.277	*X5*	0.125	0.028	0.080	0.121	0.183
X6	0.258	0.024	0.229	0.256	0.294	*X6*	0.160	0.042	0.103	0.162	0.220
X7	Not significant					*X7*	0.196	0.012	0.178	0.195	0.219

From Table 2, the regression coefficients in both the *2D_FD* and *3D_FD* cases exhibit similar variation characteristics. In exception for *X1*, which demonstrates a negative correlation with the dependent variable, all other independent variables display a positive correlation. The impact of each independent variable on the fractal dimensions can be assessed by examining the average and median values of regression coefficients. In the *2D_FD* case, the regression coefficients demonstrate a descending order, as follows: *X*1 < *X*5 < *X*6 < *X*2 < *X*3. Moreover, the coefficient of *X4* on *2D_FD* closely approximates that of *X*6, while the impact of *X7* on *2D_FD* is deemed statistically insignificant. In the *3D_FD* case, the regression coefficients exhibit a similar order as follows: *X1* < *X5* < *X4* < *X6* < *X7* < *X2* < *X3*. Moreover, the impact of *X3* on the dependent variable is much greater compared to other independent variables, a finding that is consistent across both 2D and 3D cases.

3.2.2. The Spatial Distribution of Regression Coefficients

The regression coefficients corresponding to the space units that pass the test are visually represented. Positive regression coefficients are depicted in red, while negative ones are indicated in blue, as illustrated in Figures 8 and 9.

The regression coefficients of the six independent variables for *2D_FD* exhibit spatial heterogeneity, as depicted in Figure 8a. The X1 factor (through-movement flow) exerts a negative influence in the northeastern direction within the outer and middle layers while demonstrating a positive impact in a limited area along the northwestern edge. However, its effect is not statistically significant in other regions.

The X2, X4, X5, and X6 variables consistently exhibit a positive impact across all grid cells, and the coefficients display a smooth spatial distribution. The impact of X2 (to-movement flow) is slightly more pronounced in the central axis compared to other districts, while X4 (administration and public services) exhibits a slightly stronger influence in the southeast districts. Moreover, X5 (business and commercial services) demonstrates a slighter dominance in the southwest, whereas X6 (manufacturing, industrial, and warehouse) displays a relatively stronger effect in the northwest.

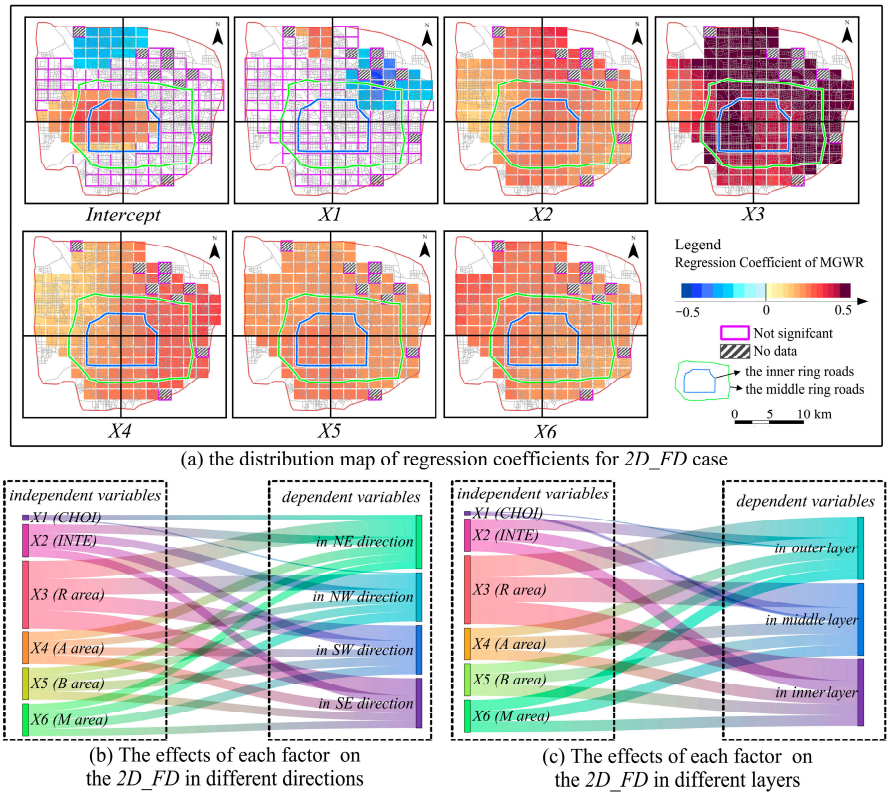

Figure 8. The distribution of regression coefficients for *2D_FD* by the MGWR method.

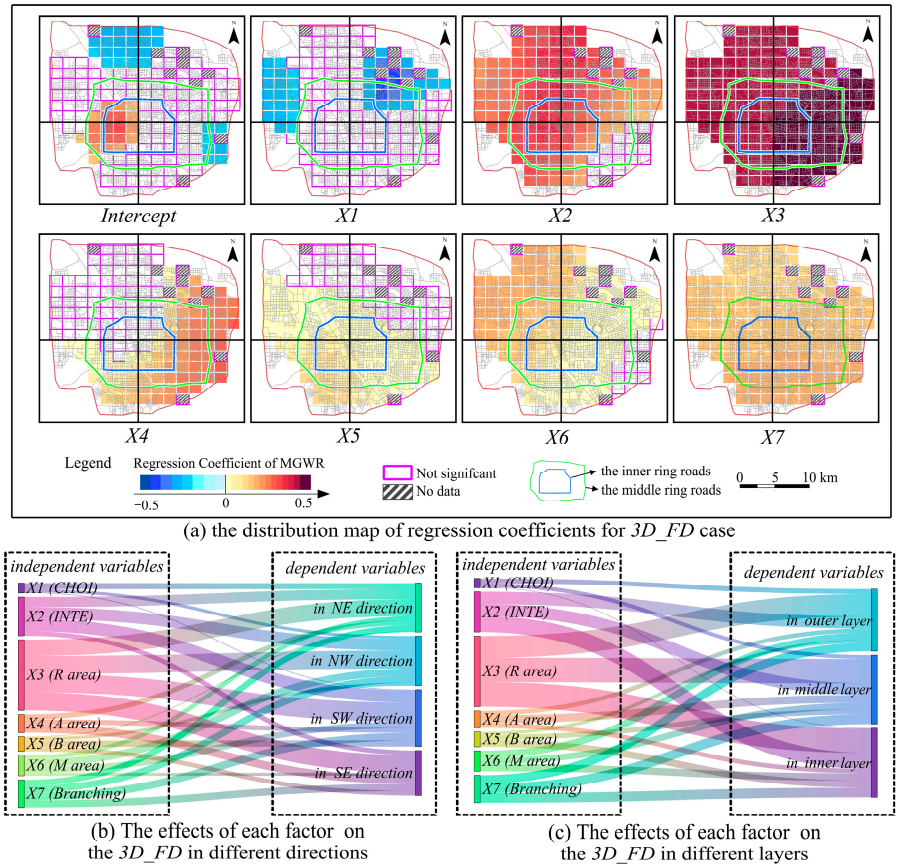

Figure 9. The distribution of regression coefficients for *3D_FD* by the MGWR method.

The X3 variable (residential area) exerts a significant influence on *2D_FD* across the majority of grids, particularly in two specific districts: one being the arc belts that extend from east to north along the middle ring roads, and the other being the western half of the inner layers.

The comparison of the contributions of different independent variables to the 2D morphology in specific directions or urban layers is depicted in Figure 8b,c, respectively. Certain similarities can be observed among the city's four directions and three circle layers. Taking the NE direction as an example, X1 exhibits a weak contribution while X3 exerts a strong impact, whereas there are only marginal disparities observed between X2, X4, X5, and X6, with their influences being moderate. Similar characteristics can also be discerned in other regions.

The impacts of the independent variables on *3D_FD* at different spatial positions exhibit variations in both magnitude and statistical significance, as indicated in Figure 9a. The X1 variable (through-movement flow) exerts a negative impact on the northeastern region beyond the inner ring roads and the western region outside the middle ring roads, while its influence in other areas lacks statistical significance. The X2 variable (to-movement flow) presents a robust positive impact in most areas of the city, particularly along the central axis. However, its significance diminishes when moving toward the southeast direction beyond the inner ring of the city. The boundary of the insignificant area in the southeast aligns with the spatial distribution of a river, namely the Qili River. This river serves as a dividing line for maintaining morphological consistency within the built environment on both sides. Furthermore, the premature development of roads on the southeastern bank has resulted in architectural incongruity and insignificance of the local regression. The X3 variable (residential area) shows a consistently strong positive impact throughout all locations, with greater intensity observed in southeastern sectors relative to other districts. The effects of X4 (administration and public services) are only significant in the half arc located in the southeast, with strong impacts observed at the periphery and weaker influences near the center. The X5 variable (business and commercial services) exhibits a modest yet statistically significant positive impact exclusively in the urban core and the southwestern half, while its influence is not statistically significant in other regions. The X6 variable (manufacturing, industrial, and warehouse) demonstrates a significant positive impact in the majority of areas within the city, gradually diminishing in intensity from the northwest to southeast direction until it becomes statistically insignificant. The X7 variable (branching degree) displays a consistently positive impact across all grids, demonstrating less spatial variability compared to other variables.

The contributions of each variable to the four directions and three layers can be observed in Figure 9b,c. It is evident that X1 has the weakest contribution, while X3 exhibits the strongest contribution. Additionally, X2 demonstrates the second strongest contribution to most zones. The contribution rankings of X3 to X7 vary across different directions and layers as detailed below. In the NE and SW directions, X7 exhibits a greater magnitude than X4, which in turn surpasses X6 and X5. In the NW direction, X6 exceeds both X7 and X5 (with X4 being insignificant). In the SE direction, it is observed that X4 surpasses both X7 and X5 before being surpassed by X6. Additionally, across all three layers, there is a consistent pattern: the magnitudes follow the order of importance as follows: X7 > X6 > X4 > X5.

4. Discussion

4.1. Discussion of the Fractal Measurement at the Subzone Level

The fractal dimension, whether in natural systems [42–44] or man-made systems like cities, is a complex object characterized by a specific spatial order generated through recursive iteration rules [45,46]. It presents inherent self-similarity at both the macro and micro levels. In the context of urban systems, the fractal dimension serves as a scientific tool for measuring the features of urban morphology and its evolutionary patterns. Moreover, it serves as a crucial indicator for evaluating whether a city is undergoing self-organizational evolution or is in a state of 'chaos' [47]. The findings of previous research indicate that self-

organized urban systems exhibit significant fractal characteristics, which can be quantified through 2D or 3D fractal dimensions [48]. However, previous studies have only employed these two fractal dimensions to examine the overall fractal characteristics of the entire city, without conducting more refined fractal measurements for subzones in different directions and urban layers.

One of the significant findings made in this study lies in the discovery of the existence of a fractal structure at the subzone level in a city, serving as an analogy and supplement to previous research findings on the overall fractal rules observed in other cities [2]. In contrast to previous studies, this discovery provides support for the spatial heterogeneity of distinct subzone structures through varying *2D_FD* or *3D_FD* values. The reason lies in the divergent planning and development trajectories of different subzones, as well as the disparities in spatial occupation and utilization method by the population, land, and architecture across urban blocks. As the box-counting dimension indicates the spatial occupancy capacity, urban growth will lead to an increase in the box-counting dimension. That is, the self-organizational goal of urban development is to optimize the spatial configuration and facilitate coordinated growth within its internal areas, thus enhancing spatial occupying efficiency and compactness while achieving a more balanced and efficient distribution of urban space. The study enriches the theory of fractal cities by demonstrating a gradual decline in the fractal dimension from the city's core to its outskirts, indicating outward expansion. Moreover, it reveals that mature subzones exhibit higher fractal dimensions compared to those in the developmental stage or undergoing rapid development.

4.2. Discussion of the Pattern of Influencing Factors for Urban Morphology

Urban morphology can be visually manifested through the architectural layout, which is undeniably interconnected with road network patterns and land-use patterns [49–51]. The former serves as the fundamental framework of urban infrastructure, while the latter plays a pivotal role in determining building functions. Moreover, the spatial arrangement of the architecture is inevitably constrained by the site if it is considered as occupancy within the road network or land parcels [52]. However, earlier studies have not explicitly explored the influence on urban fractal characteristics.

(1) The influencing pattern of the road network.

This empirical study enables the establishment of a theoretical correlation between space syntax and fractal dimension within urban areas, which has never been explored by previous research, and will offer valuable insights for urban spatial studies in the future. In the spatial syntax framework, the characteristic index of the road network is categorized into *choice* degree and *integration* degree, which correspond to two distinct traffic modes: through-movement and to-movement. The role of through-movement traffic in the completely built-up area of the city is not significant, possibly due to its primary reflection on the road section's "channel" function rather than adequately capturing the attractiveness of socioeconomic activities, thus exerting a lesser influence on urban morphology. The impact of to-movement traffic is relatively positive, potentially due to its embodiment of the road section's centrality. It can be deduced that the impact of to-movement on urban fractal dimension is a gradual process that occurs in conjunction with the progress of urban development. The influencing mechanism can be explained by the fact that a higher value of to-movement in a particular area enhances its attractiveness for socioeconomic activities, particularly where an important road extends but the land remains undeveloped. Consequently, the given plot will experience an increased influx in architecture filling, exhibiting a heightened level of self-organization aimed at optimizing urban space utilization and further augmenting the fractal characteristics.

(2) The influencing pattern of land use.

The impact of the four types of land use on *2D_FD* is more significant and demonstrates greater spatial heterogeneity in comparison to *3D_FD*, respectively. This can be interpreted as follows: the 2D arrangement of architectures on a plot boundary is constrained and coordinated with the land-use layout, while the 3D morphological characteristics of ar-

chitectures exhibit a certain degree of freedom from these constraints, resulting in greater variation in height.

The influencing mechanism of land use on fractal characteristics can be elucidated through the lens of architectural functions. In particular, land use determines the building function type within a given area, thereby exerting a profound influence on the 2D and 3D architectural layouts. This paper examines four typical land-use types and selects a representative plot for each type (Figure 10) to provide an illustrative example. ① Residential areas have the most significant impact on the fractal characteristics of urban morphology. This is due to their extensive distribution and large spatial coverage within a city. Additionally, residential buildings exhibit distinct voxel characteristics with predominantly square shapes, displaying regular arrangements and well-organized clusters (Figure 10a). These factors constitute the primary mechanism through which residential functions shape urban morphology. ② The influence of administration and public facilities, as well as manufacturing land, on urban morphology is considered secondary, with minimal disparity between them. Public facilities encompass structures such as stadiums, libraries, and museums while manufacturing land includes buildings such as factories and logistics parks. These buildings all exhibit characteristics of large sizes and intricate designs (Figure 10b,c) to fulfill internal functional requirements, corresponding to the medium fractal dimension. ③ The impact of the business area on the fractal dimension is relatively limited, primarily due to its open layout configuration. To enhance commercial vitality and promote pedestrian flow, it is imperative for commercial buildings to consider the connectivity between the building site and the surrounding street area. Moreover, several buildings often enclose vacant spaces in various forms to create commercial clusters (Figure 10d), resulting in a correspondingly lower fractal dimension.

Figure 10. Typical architectures with different functions in Zhengzhou.

The above supports the key findings and implications that there exists a strong correlation between the influencing effects of land use, architecture functions, and fractal dimension, contributing to the field of urban morphology regulation and control through a combined view of "function and form".

4.3. Limitations

This study possesses several limitations and can be enhanced in the subsequent areas: (1) The spatial grid serves as the fundamental research sample in this paper, and determining an appropriate unit size is of utmost importance. When the analyzing unit is too small, it further disrupts the integrity of urban plots and building groups, making it

challenging to establish a comprehensive architectural group system within a single grid. The explanatory power of the independent variables will decrease by approximately 20% if the grid size is halved based on the preliminary research. Conversely, when the unit size is overly large, it fails to generate sufficient samples, as the presence of more than 140 grids is crucial in order to meet the requirement that the number of spatial samples exceeds 20 times the independent variables. Thereby, the sensitivity analysis of the model's accuracy, influenced by variations in unit size, will contribute to a deeper understanding of urban morphology in the future. (2) The present study solely focuses on the analysis of a specific time period. Urban development is a dynamic process, and the fractal dimension as well as its influencing factors may vary across different stages of urban development. The proposed future research endeavor involves the collection of multiple sets of historical maps at 5-year intervals to construct a multi-dimensional data structure with spatiotemporal attributes. Then, we suggest incorporating time dimension attributes to enhance the GWR method, known as GTWR (geographical and temporal weighted regression) [53], for a dynamic urban development situation. (3) The research area serves as an exemplary illustration of a metropolitan city characterized by a polycentric geographical structure and concentric road networks. To validate our theoretical framework, further empirical investigations are imperative to apply the model to other cities exhibiting analogous spatial configurations.

5. Conclusions

In this paper, fractal measurement of urban morphology and analysis of its influencing factors are conducted at the subzone scale using quantitative urban research methods such as fractal geometry, spatial syntax, and MGWR. Based on the obtained results and subsequent discussions, the following conclusions can be drawn: (1) At the sub-area level, both 2D and 3D configurations of urban morphology exhibit fractal characteristics, demonstrating a self-organized spatial arrangement of architectural elements within the urban environment. (2) The local fractal features of urban configurations present spatial heterogeneity, with the efficiency of the architectural layout diminishing as one moves from the city center toward the urban outskirts. (3) The fractal characteristics of urban morphology in both 2D and 3D are significantly influenced by the road network and land-use distribution. Furthermore, the influencing pattern on urban fractal features varies spatially and is regulated by distinct architectural functions.

The research conclusions contribute to clarifying the theoretical relationship between architectural layout and the complex structure of "road networks & land use", thereby enabling more effective application of architectural design practices tailored to diverse urban functions such as residential, public service, commercial, and industrial sectors.

Author Contributions: Conceptualization, C.Z. and Q.F.; methodology, C.Z. and X.P.; software, X.P.; validation, C.Z., X.P. and Q.F.; formal analysis, X.P.; investigation, X.P. and C.L.; resources, Q.F.; data curation, C.L.; writing—original draft preparation, C.L.; writing—review and editing, C.Z.; visualization, X.P.; supervision, C.Z.; project administration, C.L.; funding acquisition, C.Z. and Q.F. All authors have read and agreed to the published version of the manuscript.

Funding: This research was funded by the Natural Science Foundation of Henan Province, grant number 232300421402, and the Henan Provincial Key R&D and Promotion Special Project (Science and Technology Tackling), grant number 222102320064.

Data Availability Statement: The data presented in this study are available upon request to the corresponding author.

Conflicts of Interest: The authors declare no conflicts of interest.

References

1. Takayasu, H. *Fractals in the Physical Sciences*; Manchester University Press: Manchester, UK, 1990.
2. Chen, Y. Fractal Modeling and Fractal Dimension Description of Urban Morphology. *Entropy* **2020**, *22*, 961. [CrossRef] [PubMed]
3. Batty, M. The size, scale, and shape of cities. *Science* **2008**, *319*, 769–771. [CrossRef]
4. Batty, M.; Longley, P.A. The fractal simulation of urban structure. *Environ. Plann. A* **1986**, *18*, 1143–1179. [CrossRef]

5. Benguigui, L.; Marinov, M.; Portugali, Y. When and where is a city fractal? *Environ. Plann. B-Urban* **2000**, *27*, 507–519. [CrossRef]
6. Feng, J.; Chen, Y. Spatiotemporal evolution of urban form and land-use structure in Hangzhou, China: Evidence from fractals. *Environ. Plann. B-Urban* **2010**, *37*, 838–856. [CrossRef]
7. Yin, J. Dynamical fractal: Theory and case study. *Chaos Soliton. Fract.* **2023**, *176*, 114190. [CrossRef]
8. Mandelbrot, B. *The Fractal Geometry of Nature*; W. H. Freeman and Company: New York, NY, USA, 1983.
9. Chen, Y. Derivation of the functional relations between fractal dimension of and shape indices of urban form. *Comput. Environ. Urban* **2011**, *35*, 442–451. [CrossRef]
10. Tannier, C.; Thomas, I. Defining and characterizing urban boundaries: A fractal analysis of theoretical cities and Belgian cities. *Comput. Environ. Urban* **2013**, *41*, 234–248. [CrossRef]
11. Frankhauser, P.; La, F. *Structures Urbaines (The Fractal Aspects of Urban Structures)*; Economica, Anthropos: Paris, France, 1994.
12. Carmen, G.; Jesús, S. Covering fractals with constant radius tiles: Distribution functions and their implications for resource management. *Chaos Soliton. Fract.* **2021**, *143*, 110626.
13. Chen, Y. Fractal analytical approach of urban form based on spatial correlation function. *Chaos Soliton. Fract.* **2013**, *49*, 47–60. [CrossRef]
14. Chen, L.; Feng, R.; Wang, L. Fractal Characteristic Analysis of Urban Land-Cover Spatial Patterns with Spatiotemporal Remote Sensing Images in Shenzhen City (1988–2015). *Remote Sens.* **2021**, *13*, 4640. [CrossRef]
15. Tara, A.; Patuano, A.; Lawson, G. Between 2D and 3D:Studying Structural Complexity of Urban Fabric Using Voxels and LiDAR-Derived DSMs. *Fractal Fract.* **2021**, *5*, 227. [CrossRef]
16. Sui, L.; Wang, H.; Wu, J.; Zhang, J.; Yu, J.; Ma, X.; Sun, Q. Fractal Description of Rock Fracture Networks Based on the Space Syntax Metric. *Fractal Fract.* **2022**, *6*, 353. [CrossRef]
17. Deng, H.; Wen, W.; Zhang, W. Analysis of Road Networks Features of Urban Municipal District Based on Fractal Dimension. *ISPRS Int. J. Geo-Inf.* **2023**, *12*, 188. [CrossRef]
18. Wang, J.; Lu, F.; Liu, S. A classification-based multifractal analysis method for identifying urban multifractal structures considering geographic mapping. *Comput. Environ. Urban* **2023**, *101*, 101952. [CrossRef]
19. Guo, J.; Han, G.; Xie, Y.; Cai, Z.; Zhao, Y. Exploring the relationships between urban spatial form factors and land surface temperature in mountainous area: A case study in Chongqing city, China. *Sustain. Cities Soc.* **2020**, *61*, 102286. [CrossRef]
20. Boeing, G. Spatial information and the legibility of urban form: Big data in urban morphology. *Int. J. Inform. Manag.* **2021**, *56*, 102013. [CrossRef]
21. Kulcke, M.; Lorenz, W. Spherical Box-Counting: Combining 360° Panoramas with Fractal Analysis. *Fractal Fract.* **2023**, *7*, 327. [CrossRef]
22. Dawes, M.; Ostwald, M.; Lee, J. The Mathematics of 'Natural Beauty' in the Architecture of Andrea Palladio and Le Corbusier: An Analysis of Colin Rowe's Theory of Formal Complexity Using Fractal Dimensions. *Fractal Fract.* **2023**, *7*, 139. [CrossRef]
23. Katona, V. The Hidden Dimension of Facades: Fractal Analysis Reveals Composition Rules in Classical and Renaissance Architecture. *Fractal Fract.* **2023**, *7*, 257. [CrossRef]
24. Tian, J.; Yu, M.; Ren, C.; Lei, Y. Network-scape metric analysis: A new approach for the pattern analysis of urban road networks. *Int. J. Geogra Inf. Sci.* **2018**, *33*, 537–566. [CrossRef]
25. Xu, J. From walking buffers to active places: An activity-based approach to measure human-scale urban form. *Landsc. Urban Plan* **2019**, *191*, 103452. [CrossRef]
26. Shi, B.; Yang, J. Scale, distribution, and pattern of mixed land use in central districts: A case study of Nanjing, China. *Habitat Int.* **2015**, *46*, 166–177. [CrossRef]
27. Meng, Y.; Xing, H. Exploring the relationship between landscape characteristics and urban vibrancy: A case study using morphology and review data. *Cities* **2019**, *95*, 102389. [CrossRef]
28. Yunitsyna, A.; Shtepani, E. Investigating the socio-spatial relations of the built environment using the Space Syntax analysis—A case study of Tirana City. *Cities* **2022**, *133*, 104147. [CrossRef]
29. Serra, M.; Hillier, B. Angular and Metric Distance in Road Network Analysis: A nationwide correlation study. *Comput. Environ. Urban* **2019**, *74*, 194–207. [CrossRef]
30. Yang, X.; Chen, X.; Qiao, F.; Che, L.; Pu, L. Layout optimization and multi-scenarios for land use: An empirical study of production-living-ecological space in the Lanzhou-Xining City Cluster, China. *Ecol. Indic.* **2022**, *145*, 109577. [CrossRef]
31. Wu, C.; Ye, Y.; Gao, F.; Ye, X. Using street view images to examine the association between human perceptions of locale and urban vitality in Shenzhen, China. *Sustain. Cities Soc.* **2023**, *88*, 104291. [CrossRef]
32. Guo, F.; Schlink, U.; Wu, W.; Mohamdeen, A. Differences in Urban Morphology between 77 Cities in China and Europe. *Remote Sens.* **2022**, *14*, 5462. [CrossRef]
33. Ma, X.; Zhang, J.; Ding, C.; Wang, Y. A geographically and temporally weighted regression model to explore the spatiotemporal influence of built environment on transit ridership. *Comput. Environ. Urban* **2018**, *70*, 113–124. [CrossRef]
34. Yang, Y.; Fu, B. Spatial Heterogeneity of Urban Road Network Fractal Characteristics and Influencing Factors. *Sustainability* **2023**, *15*, 12141. [CrossRef]
35. Frankhause, P. The fractal approach: A new tool for the spatial analysis of urban agglomerations. *Popul. Engl. Sel.* **1998**, *10*, 205–240.

36. Zhang, H.; Lan, T.; Li, Z. Fractal evolution of urban street networks in form and structure: A case study of Hong Kong. *Int. J. Geogra Inf. Sci.* **2022**, *36*, 1100–1118. [CrossRef]
37. Hillier, B. *Space Is the Machine: A Configurational Theory of Architecture*; Cambridge University Press: Cambridge, UK, 1996.
38. Fotheringham, W.; Yang, W.; Kang, W. Multiscale Geographically Weighted Regression (MGWR). *Ann. Am. Assoc. Geogr.* **2017**, *107*, 1247–1265. [CrossRef]
39. Wu, J.; Tu, Y.; Chen, Z.; Yu, B. Analyzing the Spatially Heterogeneous Relationships between Nighttime Light Intensity and Human Activities across Chongqing, China. *Remote Sens.* **2022**, *14*, 5695. [CrossRef]
40. Oshan, T.M.; Li, Z.; Kang, W.; Wolf, L.J.; Fotheringham, A.S. MGWR: A Python Implementation of Multiscale Geographically Weighted Regression for Investigating Process Spatial Heterogeneity and Scale. *ISPRS Int. J. Geo-Inf.* **2019**, *8*, 269. [CrossRef]
41. Al-Sayed, K.; Turner, A.; Hillier, B.; Lida, S.; Penn, A. *Space Syntax Methodology*; Bartlett School of Architecture, UCL: London, UK, 2014.
42. Jin, Y.; Liu, X.; Song, H.; Zheng, J.; Pan, J. General fractal topography: An open mathematical framework to characterize and model mono-scale-invariances. *Nonlinear Dyn.* **2019**, *96*, 2413–2436. [CrossRef]
43. Huang, J.; Kim, J.; Agrawal, N.; Sudarsan, A.P.; Maxim, J.E.; Jayaraman, A.; Ugaz, V.M. Rapid fabrication of bio-inspired 3D microfluidic vascular networks. *Adv. Mater.* **2009**, *21*, 3567–3571. [CrossRef]
44. Lim, A.E.; Goh, S. Effect of Microchannel Diameter on Electroosmotic Flow Hysteresis. *Energies* **2023**, *16*, 2154. [CrossRef]
45. Arseniou, G.; MacFarlane, D.W.; Seidel, D. Woody Surface Area Measurements with Terrestrial Laser Scanning Relate to the Anatomical and Structural Complexity of Urban Trees. *Remote Sens.* **2021**, *13*, 3153. [CrossRef]
46. Li, Z.; Zhao, W.; Nie, M. Scale Characteristics and Optimization of Park Green Space in Megacities Based on the Fractal Measurement Model: A Case Study of Beijing, Shanghai, Guangzhou, and Shenzhen. *Sustainability* **2021**, *13*, 8554. [CrossRef]
47. Man, X.; Chen, Y. Fractal-Based Modeling and Spatial Analysis of Urban Form and Growth: A Case Study of Shenzhen in China. *ISPRS Int. J. Geo-Inf.* **2020**, *9*, 672. [CrossRef]
48. Song, Z.; Jin, W.; Jiang, G.; Li, S.; Ma, W. Typical and atypical multifractal systems of urban spaces—Using construction land in Zhengzhou from 1988 to 2015 as an example. *Chaos Solitons Fractals* **2021**, *145*, 110732. [CrossRef]
49. Christopher, S. Multisensor Characterization of Urban Morphology and Network Structure. *Remote Sens.* **2019**, *11*, 2162.
50. Ossola, A.; Locke, D.; Lin, B.; Minor, E. Greening in style: Urban form, architecture and the structure of front and backyard vegetation. *Landsc. Urban Plan* **2019**, *185*, 141–157. [CrossRef]
51. Wu, J.; Wang, S.; Zhang, Y.; Zhang, A.; Xia, C. Urban landscape as a spatial representation of land rent: A quantitative analysis. *Comput. Environ. Urban* **2019**, *74*, 62–73. [CrossRef]
52. Wentz, E.A.; York, A.M.; Alberti, M.; Conrow, L.; Fischer, H.; Inostroza, L.; Jantz, C.; Pickett, S.T.; Seto, K.C.; Taubenböck, H. Six fundamental aspects for conceptualizing multidimensional urban form: A spatial mapping perspective. *Landsc. Urban Plan* **2018**, *179*, 55–62. [CrossRef]
53. Zhao, M.; Wang, H.; Sun, J.; Tang, R.; Cai, B.; Song, X.; Huang, X.; Huang, J.; Fan, Z. Spatio-temporal characteristics of soil Cd pollution and its influencing factors: A Geographically and temporally weighted regression (GTWR) method. *J. Hazard. Mater.* **2023**, *446*, 130613. [CrossRef] [PubMed]